International Journal of Mechanical, Industrial and Aerospace Sciences
ISSN: 2517-9950
Vol:6, No:7, 2012

Incident Shock Wave Interaction with an Axisymmetric Cone Body Placed in Shock Tube

Rabah Haoui

***Abstract*—**This work presents a numerical simulation of the interaction of an incident shock wave propagates from the left to the right with a cone placed in a tube at shock. The Mathematical model is based on a non stationary, viscous and axisymmetric flow. The Discretization of the Navier-stokes equations is carried out by the finite volume method in the integral form along with the Flux Vector Splitting method of Van Leer. Here, adequate combination of time stepping parameter, CFL coefficient and mesh size level is selected to ensure numerical convergence. The numerical simulation considers a shock tube filled with air. The incident shock wave propagates to the right with a determined Mach number and crosses the cone by leaving behind it a stationary detached shock wave in front of the nose cone. This type of interaction is observed according to the time of flow. 02122367929

***Keywords*—**Supersonic flow, viscous flow, finite volume, cone body, shock wave

I. Introduction

THE conventional shock tube consists of a duct of constant cross-section separated by a diaphragm into a high pressure or driver section and a low pressure or driven section (fig. 1). When the diaphragm is ruptured, a shock wave is generated which propagates into the low pressure region, accelerating the gas and raising its temperature. Simultaneously an expansion wave propagates into the high pressure region, accelerating the driver gas into the driven section. The flow regions induced behind these waves are separated by an interface or contact surface across which the pressure and velocity are equal, whilst the density and temperature are in general different. Between the incident shock wave and the interface there exists a short duration of compressed quasi-steady flow and heated gas which is available for test purposes. The theory and operation of shock tubes have been well reported in the literature theory Shapiro [1] and therefore not detailed here.

With an unsteady scheme, the flow inside the tube shock (fig.2) is simulated by presenting a diagram($x[m], t[ms]$). On the figure of right-hand side which represents contours of pressure, one observes the incident shock wave which propagates on the right with a constant supersonic speed then it is reflected on the bottom of the tube shock. Expansion waves propagate on the left in the driven tube and then are reflected on the wall. The smoothness of curves provides a mean to prove the precision of calculations and the consistency of our code. The figure of left represents the density contours of gas. The separation surface is observed between the incident shock wave and the expansion waves.

Rabah Haoui is whit Department of Mechanical and Engineering, University of Science and Technology, Algiers, Algeria. (fax: 00.213.21.20.77.65 ; e-mail: haoui_rabah@ yahoo.fr).

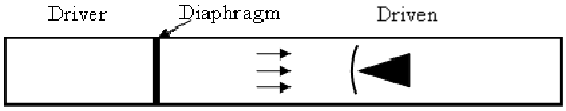

Fig. 1 shock tube

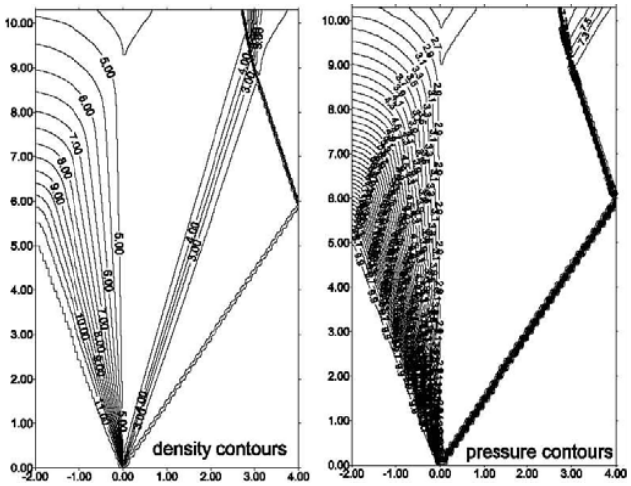

Fig. 2 Incident wave in tube shock

The problem to be treated is illustrated in Fig. 3. A plan shock wave with the Mach number $M_s = 3$ propagates from left to right and interacts with a cone whose axis is perpendicular to the shock wave front. The cone's half-angle is equal to 43°.

The gas in front of the incident shock wave is at rest with pressure of $2\,KPa$ and a temperature of $293\,K$. After the shock occurs, State 2 is determined by the laws of the moving normal shock wave. We have, $M_2 = 1\ .3\ 6 P_2 = 0\ .2\ bars$ and $T_2 = 804K$. The incident shock crosses the axisymmetric cone placed in the shock tube and at the same time a detached shock wave is formed before the cone as the incidental shock moves on the right. Then, States 1 and 2 constitute the initial solution of the problem. The numerical simulation is performed using the Navier-Stokes equations. The cone's surface is supposed to be ideally smooth.

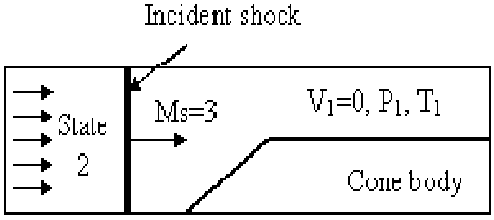

Fig. 3 Problem scheme

II. Governing of Equations

For a Newtonian fluid, the viscous stresses are proportional to the rates of deformation. The three-dimensional form of Newton's law of viscosity for compressible flows involves two constants of proportionality: the first dynamic viscosity, μ to relate stresses to linear deformations, and the second viscosity, λ to relate stresses to the volumetric deformation.

Not much is known about the second viscosity λ, because its effect is small in practice (usually, $\lambda = -\frac{2}{3}\mu$ Schlichting [2] for gases).

The Navier-stokes equations in a flux-vector form under a Cartesian coordinate system are given by

$$\frac{\partial W}{\partial t} + \frac{\partial E}{\partial x} + \frac{\partial F}{\partial y} + \frac{\partial G}{\partial z} = 0 \quad (1)$$

Where the vectors W, E, F and G are given by

$$W = \begin{pmatrix} \rho \\ \rho u \\ \rho v \\ \rho w \\ \rho e \end{pmatrix}$$

$$E = \begin{pmatrix} \rho u \\ \rho u^2 + p - \tau_{xx} \\ \rho uv - \tau_{xy} \\ \rho uw - \tau_{xz} \\ (\rho e + p)u - u\tau_{xx} - v\tau_{xy} - w\tau_{xz} + q_x \end{pmatrix}$$

$$F = \begin{pmatrix} \rho v \\ \rho uv - \tau_{xy} \\ \rho v^2 + p - \tau_{yy} \\ \rho vw - \tau_{yz} \\ (\rho e + p)v - u\tau_{xy} - v\tau_{yy} - w\tau_{yz} + q_y \end{pmatrix}$$

$$G = \begin{pmatrix} \rho w \\ \rho uw - \tau_{xz} \\ \rho vw - \tau_{yz} \\ \rho w^2 + p - \tau_{zz} \\ (\rho e + p)w - u\tau_{xz} - v\tau_{yz} - w\tau_{zz} + q_z \end{pmatrix}$$

The heat flux vector q has three components q_x, q_y and q_z given by the Fourier's law of heat conduction relates the heat flux to the local temperature gradient. So

$$q_x = -k\frac{\partial T}{\partial x},\ q_y = -k\frac{\partial T}{\partial y},\ q_z = -k\frac{\partial T}{\partial z} \quad (2)$$

Where k denotes the coefficient of thermal conductivity, it is function of Prandtl number, viscosity and specific heat.

$$k = Cp.\mu/Pr \quad (3)$$

The energy per unit of mass e is defined as the sum of the internal energy and the kinetic energy as

$$e = c_v T + \frac{1}{2}(u^2 + v^2 + w^2) \quad (4)$$

III. Axisymmetric Formulation

We do not lose general information by seeking the solution at the points of an infinitely small domain. A method developed within the Sinus project of the INRIA Sophia-Antipolis, Goudjo and Désidéri [3] makes it possible to pass from 3D to 2D axisymmetric by using a technique known as disturbance of domain. In the present work, and taking advantage of such simplification, our 3D model is considered axisymmetric (see details. in haoui [4]).

IV. Discretization In Time

The present numerical method is based on an explicit approach in time and space. The step of time Δt is such as:

$$\Delta t_{i,j} = min\left[\left(\frac{\Delta x.CFL}{\|V\|+a}\right), \left(\frac{(\Delta x)^2.CFL}{2\mu}\right)\right] \quad (5)$$

The *CFL* (Courant, Friedrich, Lewis) is a stability factor Hoffmann [5]. V is the velocity of the flow and a is the speed of sound. Δx is the small length of the mesh at the same point (i, j).

The choice of the grid plays an important role in determining in the convergence of calculations. Therefore, it is indeed advisable to have sufficiently refine meshes at the places where the gradients of the flow parameters are significantly large haoui [4].

V. Decomposition of Van-Leer

In this study, the decomposition of Van-Leer [6] is selected, namely a decomposition of flows in two parts f_{VL}^- and f_{VL}^+ .This decomposition must apply to the present two-dimensional problem by calculating the flow within each interface between two cells. Moreover, through the interface, the normal direction is paramount, thus, a change of reference mark is applied to place in the reference mark of the interface and its normal by the intermediary of a rotation $\boldsymbol{R}$. This decomposition technique has been throughly and successfully tested for a supersonic flow around a blunt body, haoui [10].

Moreover, at each interface $(i + 1/2)$, two neighbor states (i) and $(i + 1)$ are known. Thus, one can calculate the one-dimensional flow F through the interface, total flow $f(W, \eta)$ being deduced from F by applying the opposite rotation, as:

$$f(W, \vec{\eta}) = \|\vec{\eta}\|.\boldsymbol{R^{-1}}\left(F(W^R)\right) \quad (6)$$

This property makes it possible to use only one component of flow f (F for example) to define the decomposition of flow in two dimensions. Moreover, this method is much easy and simple to implement than the decomposition of flow in two dimensions $f = F\eta_x + G\eta_y$.

Similarly, the expressions of $F_{VL}^+(W^R)$ and $F_{VL}^-(W^R)$, where W^R is defined as the transform of W by rotation $\boldsymbol{R}$, see haoui [4,8 and10].

VI. Boundary Conditions

Open (far field) boundary conditions are the most challenging numerical problem encountered in developing general CFD codes. CFD problems are defined in terms of initial and boundary conditions, and thus it is important to specify these correctly and understand their role in the

numerical algorithm. In transient problems, the initial values of all the flow variables need to be specified at all solution points in the flow domain. Since this involves no special measures other than initializing the appropriate data arrays we do not need to discuss this topic further. The present work describes the implementation of the most common boundary conditions in the discredited equations of the finite volume method, namely: inlet, outlet, wall and symmetry axis.

A. Inlet boundary conditions

At the inlet the pressure and temperature are fixed, they are the flow parameters behind the incidental shock wave setting.

B. Body surface

The no-slip condition for the velocity is usually used at the body surface, cone and tube. The temperature gradient at the wall is zero, in accordance with the Fourier equation of heat conduction in the y-direction together with the assumption of zero heat flux at the wall. In the present study, the temperature at the wall is not very different of the stagnation temperature of free stream. The wall shear stress is calculated by:

$$\tau_w = \mu \left(\frac{\partial v_t}{\partial n}\right)_{wall} \quad (7)$$

Here we assume that the coordinate of the unit vector t is in the direction of the shear force at the wall and the unit vector n is normal at t, Ferziger [7].

C. Axis of symmetry

The conditions of symmetry at the boundary are: (i) no flow across the boundary and (ii) no scalar flux across the boundary.

D. Outlet boundary conditions

At the exit of the computational domain, the flow parameters are extrapolated from the interior values, let us note that the shock wave does not have attaint yet the exit of the field and state 1 is always maintained.

VII. Results and Interpretations

A flow around an axisymmetric cone body placed in tube shock is used as a benchmark. The figure 4 shows the domain of calculation with a grid of (117 x 21). Note that our calculations are based on a grid of (1481 x 252), as numerical accuracy is related to the choice of the grid size haoui [9, 10]. The gas used is the fresh air. The initial solution is established with state 1 and state 2 separate at $x_s = -24mm$. Figure 5 shows the evolution of the Mach contours in function of time.

At $t = 0$, an incident shock wave is propagated with a Mach number $M_s = 3$. Note that at $t = 2\mu s$, the shock wave is already advanced, as expected with the formation of the boundary layer near the wall of shock tube.

When $t = 5\mu s$, the shock reaches the nose of the cone, whilst the flow behind the shock is supersonic of which the Mach number is equal to 1.36.

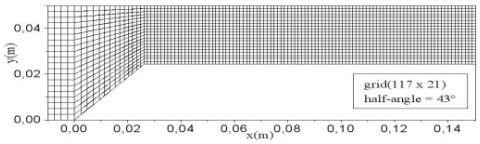

Fig. 4 Computational domain

At $t = 10\mu s$, the shock starts to cross the cone, one observes near the wall of the cone the formation of a new shock wave, round-off, connected to the incident shock. The boundary layer continues to form on the wall of the shock tube. At $t = 15\mu s$, the incident shock advances and a detached shock starts to form. It is clear at $t = 20\mu s$; the incident shock wave remains normal since the flow before and after is one-dimensional. At $t = 25\mu s$, the shock has reached the convex part of the cone. The detached shock becomes more apparent and a two-dimensional flow takes place between the detached shock and the cone with the presence of a boundary layer on the wall of the cone.

At $t = 30\ \mu s$, expansion waves start to be formed on the convex part of the cone body while a depression takes place delaying the incident shock wave.

When $t = 40\mu s$, the detached shock wave becomes dominant, the flow between the deformed incident shock and the detached shock is completely two-dimensional. At $t = 60\mu s$, the detached shock wave interacts with the boundary layer on the wall of the shock tube, causing its reflection. Finally, at $t = 90\mu s$, the detached shock wave becomes stationary, with a determined position at $x_d = -3mm$. The incident shock continues to move on the right without disturbing the detached shock wave. One can also observe the formation of a shock lambda (λ) to the position where the interaction of the detached shock wave and the boundary layer on the wall of the shock tube takes place.

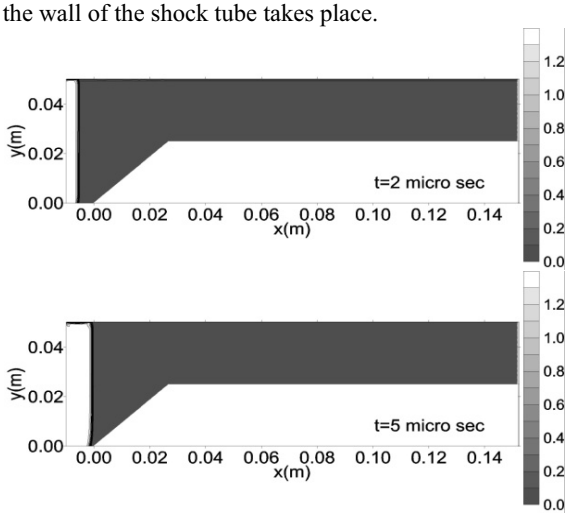

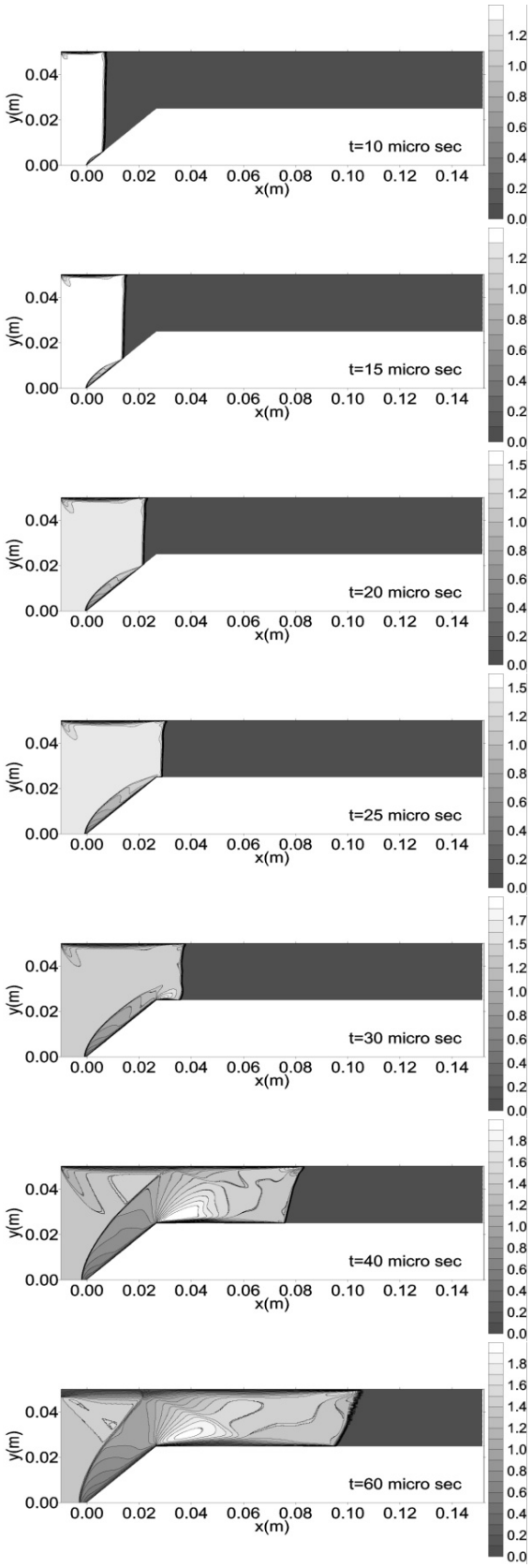

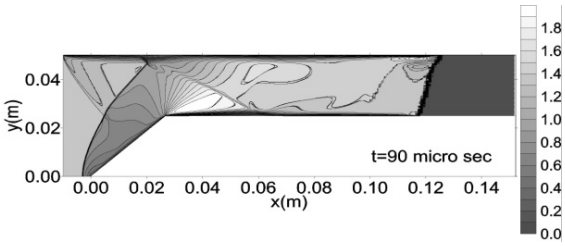

Fig. 5 Flow evolution

A detailed analysis at $t = 20\mu s$ of figure (fig. 6) shows clearly how the incident shock propagates in the shock tube while crossing the cone. Moreover, the figure also depicts the formation of detached shock and the presence of a boundary layer (B.L) both on the wall of the cone and the shock tube.

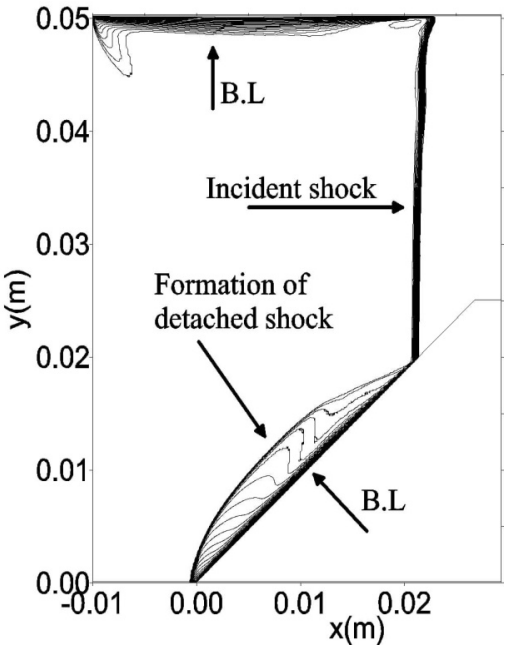

Fig. 6 Mach contours at $t = 20\mu s$

The density distribution along the axis of symmetry and on the wall of the cone is illustrated in (fig. 7). Before the cone the detached shock wave is localized with at $x_d = -3mm$, the ratio of the density increases to 4.66, causing a fast deceleration of the flow. The presence of the boundary layer provokes further increase to the ratio of density to 21.4. On the convex part of the cone, a fast falls of density and thus pressure is observed, generating expansion waves. At the distance $x = 0.06m$, an increase of density and pressure is observed, due to the interaction of the reflected shock wave with the boundary layer on the wall of the cone, this interaction is depicted on the Mach contours at $t = 90\mu s$ and $x = 0.06m$. From this station, a reduction of density is observed when the expansion waves arrive on the wall of the shock tube. On right-hand side, the incident shock wave continues its propagation.

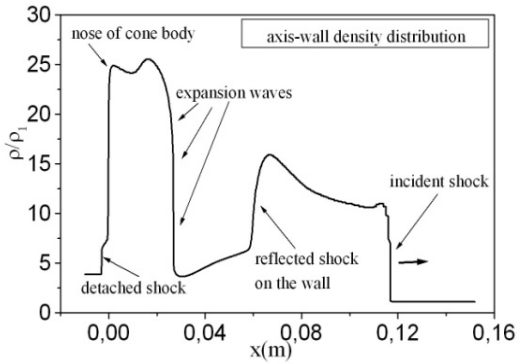

Fig. 7 Density distribution

Figure 8 illustrates horizontal velocity profile according to the radius, in particular at $x = 0.0267m$ just before the convexes part of cone body. One can clearly observe the velocity increases from zero on the wall at $y = 0{,}02489m$ to $630\ m/s$ at$y = 0{,}02731m$, resulting in the development of the boundary layer of $\delta = 2.42mm$ thickness . The flow remains almost uniform until the arrival of the reflected shock wave causes a small disturbance at$y = 42.8mm$. Thus the velocity decreases rapidly in the boundary layer on the wall of the shock tube until where it is cancelled.

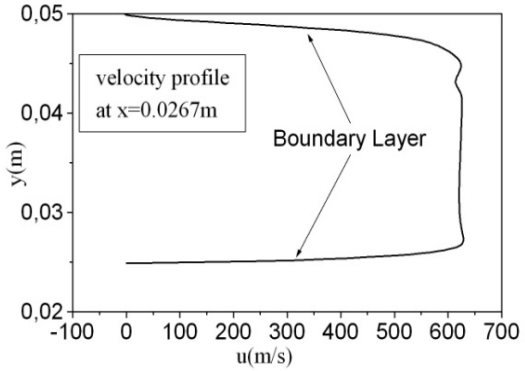

Fig. 8 Velocity profile at $x = 26.7mm$

VIII. Conclusion

The study of the flow in a tube at shock with conical shape is undertaken as a benchmark to expose the accuracy of the computational modeling of Navier-stokes equations in capturing the physics of such flow. The numerical simulation was able to capture the incident shock wave at beginning in a form of a surface of discontinuity propagating a supersonic speed, through the correct setting of the boundary conditions. The boundary layer itself was well captured near the walls with respect to the mesh size used. From view physical point, the phenomenon of the incident shock wave interaction with the cone body in the shock tube is well identified, as the incidental shock wave moves on the right, the stationary detached shock wave is formed in front of the cone during a time higher than $90\mu s$. The present model was precisely able to mimic this phenomenon observed in experimental trials.

References

[1] A.H. Shapiro, The Dynamics and Thermodynamics of Compressible fluid flow, The Ronald Press Company, New York, Volume II, 1954, pp. 664.

[2] H. Schlichting, Boundary-layer theory, 7th edition, McGraw-Hill, New York, 1979.

[3] Goudjo, J.A. Désidéri, a finite volume scheme to resolution an axisymmetric Euler equations (Un schéma de volumes finis décentré pour la résolution des équations d'Euler en axisymétrique), Research report INRIA 1005, 1989.

[4] R. Haoui, "Effect of mesh size on the viscous flow parameters of an axisymmetric nozzle," International Journal of Aeronautical and space Sciences, vol.12(2), 2011, pp. 127-133.

[5] K. A. Hoffmann, Computational fluid dynamics for engineers, Volume II. Chapter 14, Engineering Education system, Wichita, USA, pp.202-235, 1995.

[6] B. Van Leer, "Flux Vector Splitting for the Euler Equations," Lecture Notes in Physics. 170, 1982, pp. 507-512.

[7] J.H. Ferziger & all, Computational Methods for Fluid Dynamics, Chapter 8, Springer-Verlag, Berlin Heidelberg, New York, 2002, pp.217-259,.

[8] R. Haoui, "Physico-chemical state of the air at the stagnation point during the atmospheric reentry of a spacecraft," Acta astronautica, vol.68, 2011, pp.1660-1668.

[9] R. Haoui, A. Gahmousse, D. Zeitoun, "Condition of convergence applied to an axisymmetric reactive flow," 16th CFM, n°738, Nice, France, 2003.

[10] R. Haoui, "Finite volumes analysis of a supersonic non-equilibrium flow around the axisymmetric blunt body," International Journal of Aeronautical and space Sciences, vol.11(2), 2010, pp. 59-68.